SCIENTIFIC REPORTS

OPEN

Received: 11 September 2015
Accepted: 11 January 2016
Published: 15 February 2016

Thermally stable dielectric responses in uniaxially (001)-oriented $CaBi_4Ti_4O_{15}$ nanofilms grown on a $Ca_2Nb_3O_{10}^-$ nanosheet seed layer

Junichi Kimura[1], Itaru Takuwa[1], Masaaki Matsushima[1], Takao Shimizu[2], Hiroshi Uchida[3], Takanori Kiguchi[4], Takahisa Shiraishi[4], Toyohiko J. Konno[4], Tatsuo Shibata[5], Minoru Osada[5], Takayoshi Sasaki[5] & Hiroshi Funakubo[1,2]

To realize a high-temperature capacitor, uniaxially (001)-oriented $CaBi_4Ti_4O_{15}$ films with various film thicknesses were prepared on $(100)_c SrRuO_3/Ca_2Nb_3O_{10}^-$ nanosheet/glass substrates. As the film thickness decreases to 50 nm, the out-of-plane lattice parameters decrease while the in-plane lattice ones increase due to the in-plane tensile strain. However, the relative dielectric constant (ε_r) at room temperature exhibits a negligible degradation as the film thickness decreases to 50 nm, suggesting that ε_r of (001)-oriented $CaBi_4Ti_4O_{15}$ is less sensitive to the residual strain. The capacitance density increases monotonously with decreasing film thickness, reaching a value of 4.5 μF/cm^2 for a 50-nm-thick nanofilm, and is stable against temperature changes from room temperature to 400 °C irrespective of film thickness. This behaviour differs from that of the widely investigated perovskite-structured dielectrics. These results show that (001)-oriented $CaBi_4Ti_4O_{15}$ films derived using $Ca_2Nb_3O_{10}^-$ nanosheets as seed layers can be made candidates for high-temperature capacitor applications by a small change in the dielectric properties against film thickness and temperature variations.

The demand is increasing for capacitors that can function at elevated temperatures in electronic circuits in automobiles, power devices, and light-emitting diodes[1–4]. One of the most promising candidates is a ceramic capacitor due to its thermal stability. Recently, various approaches have been used to improve the performance of ceramic capacitors, including the preparation of thin-film capacitors composed of inorganic dielectrics such as perovskite-structured oxides. Although (Ba, Sr)TiO_3-based dielectrics, which have a high dielectric constant (ε_r) near room temperature, are the most widely investigated ceramic capacitor materials[5–7], they are not suitable for high-temperature capacitor applications due to their temperature instability within the required temperature range (i.e., ε_r changes drastically around the phase transition temperature). Consequently, they cannot achieve high ε_r and a small-temperature dependence of the capacitance simultaneously due to the trade-off relationship[5,7].

In addition, the ε_r of thin-film capacitors produced using (Ba, Sr)TiO_3-based materials as the dielectric layer is severely degraded as the film thickness decreases, making it difficult to enhance the capacitance density by decreasing the film thickness[8–10]. One possible reason for this sensitivity to film thickness may be the high strain sensitivity of ε_r, which remains as the film thickness decreases. These phenomena are common material problems for conventional perovskite dielectrics, suggesting that another novel capacitor material is necessary.

[1]Department of Innovative and Engineered Materials, Tokyo Institute of Technology, 4259 Nagatsuta-cho, Midoriku, Yokohama, Kanagawa 226-8502, Japan. [2]Materials Research Center for Element Strategy, Tokyo Institute of Technology, 4259 Nagatsuta-cho, Midori-ku, Yokohama 226-8503, Japan. [3]Department of Materials and Life Science, Sophia University, Chiyoda, Tokyo, 102-8554, Japan. [4]Institute for Materials Research, Tohoku University, 2-1-1 Katahira, Aoba-ku, Sendai 980-8577, Japan. [5]International Center for Materials Nanoarchitectonics (WPI-MANA), National Institute for Materials Science (NIMS), 1-1 Namiki, Tsukuba, Ibaraki, 305-0044, Japan. Correspondence and requests for materials should be addressed to H.F. (email: funakubo.h.aa@m.titech.ac.jp)

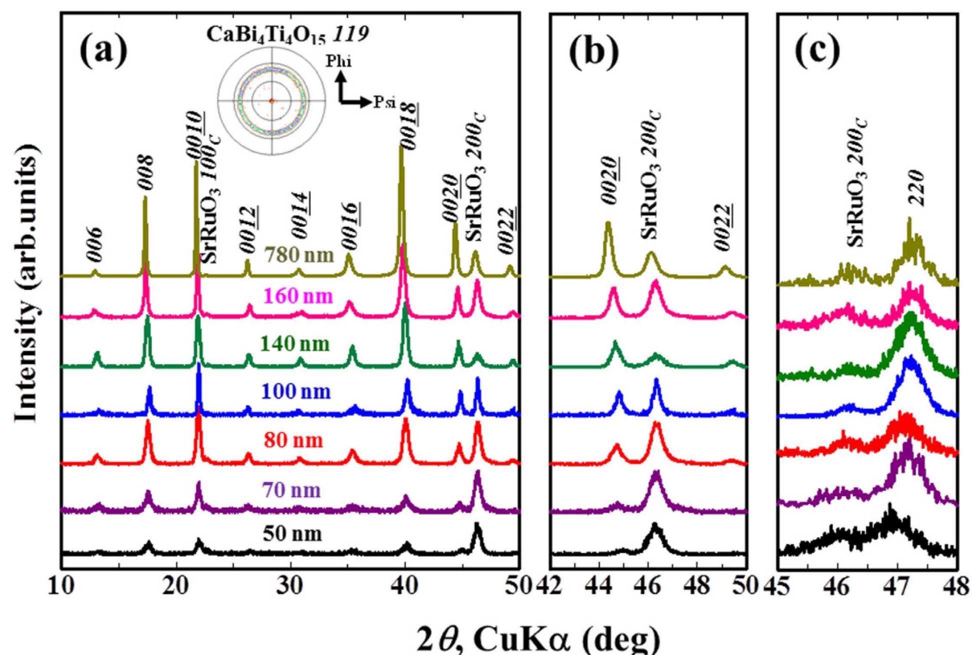

Figure 1. Out-of-plane XRD θ–2θ patterns of the films with various thicknesses in the region of (**a**) $2\theta = 10$–$50°$ and (**b**) $2\theta = 42$–$50°$ along with (**c**) the in-plane XRD θ–2θ patterns of the films in the region of $2\theta = 45$–$48°$. The inset in (**a**) shows the X-ray pole measured at a fixed 2θ angle corresponding to $CaBi_4Ti_4O_{15}$ *119* ($2\theta = 30.6°$) for 780-nm-thick films.

To realize novel dielectrics with a large capacitance density and small change in ε_r at elevated temperatures, we previously proposed bismuth layer-structured dielectrics (BLSDs)[11]. BLSDs have a natural superlattice structure along the *c*-axis [(001)-orientation], which consists of two kinds of two-dimensional monolayers (i.e., a bismuth oxide $(Bi_2O_2)^{2+}$ layer and a pseudoperovskite layer generally described as $(A_{m-1}B_mO_{3m+1})^{2-}$, where *m* is the number of BO_6 octahedra in the pseudoperovskite layer)[12,13]. Compared to $BaTiO_3$-based materials, some BLSDs exhibit a high Curie temperature and their ε_r shows small temperature dependence along the stack direction (i.e., the *c*-axis) up to the high temperature region[14–16]. These materials also have important additional features in which the degradation in ε_r as the film thickness decreases is small (i.e., a small "size effect"), allowing a high capacitance density to be realized[17]. This behaviour showing the small strain sensitivity of ε_r, which is attributed to the structural two-dimensionality of BLSDs, differs from conventional perovskite-based dielectrics.

We have already investigated the dielectric properties of 500-nm-thick (001)-oriented epitaxial films of $CaBi_4Ti_4O_{15}$, which are BLSDs prepared on $(100)_cSrRuO_3/(100)SrTiO_3$. These films not only have an ε_r of about 190 at room temperature, but they also display a stable capacitance against the applied electric field as well as temperature variations up to 500 °C[11]. Moreover, the ε_r for epitaxial thin films of $SrBi_4Ti_4O_{15}$, which is another BLSD, does not drastically degrade as the film thickness decreases to 15 nm[17]. These reports clearly show that the ε_r of thin-film capacitors of epitaxial BLSDs have a superior temperature-dependent performance compared to $BaTiO_3$-based ones and may overcome issues observed in conventional $BaTiO_3$-based materials in high-temperature applications.

However, the dielectric properties of BLSDs include a strong anisotropy due to the crystal structure of BLSDs[16]. In fact, our group has previously reported that the dependence of the film thickness on the dielectric property in BLSDs is strongly influenced by the tilting angle of the *c*-axis from the substrate normal[18]. Therefore, reproducible growth of (001)-oriented BLSDs films (i.e., the stack direction of the layers) is a critical issue to achieve a stable ε_r as both the film thickness and temperature decrease.

From the viewpoint of practical applications, reproducible fabrication of uniaxially (001)-oriented BLSDs films on various common substrates, including amorphous glasses and (100) Si wafers, is a critical issue for practical applications even if the in-plane orientation of these films is more random than that of epitaxial films. Shibata *et al.* reported the {100} orientation control of $SrTiO_3$ films on amorphous glass using a seed layer of $Ca_2Nb_3O_{10}^-$ nanosheets[19]. Based on their work, we envisioned that a $Ca_2Nb_3O_{10}^-$ seed layer could control the (001) orientation of BLSD films because (001)-oriented BLSD films were grown on (100)$SrTiO_3$ single crystals[15].

In the present study, we sought to enhance the capacitance density of Pt/(001)-oriented $CaBi_4Ti_4O_{15}/(100)_cSrRuO_3$ capacitors by decreasing the film thickness of the $CaBi_4Ti_4O_{15}$ layer. This should allow the capacitor size to be scaled down or the total capacitance to be increased. In the case of (Ba, Sr)TiO_3 film capacitors, ε_r is reported to change drastically not only with film thickness but also with temperature, which makes it difficult to design a capacitor with a small capacitance change over a wide temperature range[8–10]. For (001)-oriented $CaBi_4Ti_4O_{15}$ films, the capacitance density reaches 4.5 μF/cm^2 as the film thickness is decreased to 50 nm, and the capacitance has a small temperature coefficient from room temperature to 400 °C despite the increase in the residual strain

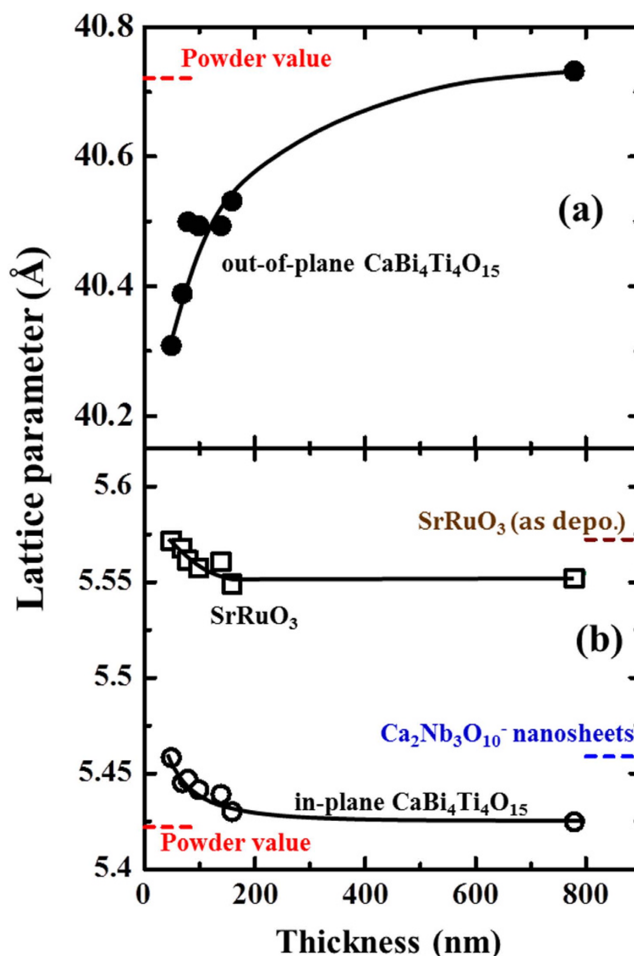

Figure 2. (**a**) Out-of-plane and (**b**) in-plane lattice parameters of the films as functions of film thickness. (●: out-of-plane; ○: in-plane). (**b**) A plot of the in-plane lattice parameter of the $SrRuO_3$ layer (□) determined from the data in Fig. 1(c) is shown. Reference data of $Ca_2Nb_3O_{10}$[19–20] are also shown.

as the film thickness decreases. The present results indicate that nanosheet-buffered uniaxially (001)-oriented $CaBi_4Ti_4O_{15}$ thin films are promising alternatives to (Ba, Sr)TiO_3-based films in high temperature capacitors.

Results and discussion

Crystal structure and microstructure. The out-of-plane XRD θ–2θ patterns for $CaBi_4Ti_4O_{15}$ films with various thicknesses show only the $h00_c$ and $00l$ diffraction peaks of $SrRuO_3$ and $CaBi_4Ti_4O_{15}$ (Fig. 1(a)), respectively, suggesting a (001) single orientation of $CaBi_4Ti_4O_{15}$ regardless of the film thickness. The X-ray pole figure measurement at a fixed 2θ angle corresponding to $CaBi_4Ti_4O_{15}$ *119* ($2\theta = 30.6°$) shows strong ring-shape-peaks at *Psi* ≑ 50° for 780-nm-thick films (inset of Fig. 1(a)), indicating a uniaxial (001)-orientation along the substrate surface normal with an in-plane random orientation.

Figure 1(b) presents the enlarged XRD patterns around the $CaBi_4Ti_4O_{15}$ *00<u>20</u>* peak in Fig. 1(a). The diffraction angles of the $CaBi_4Ti_4O_{15}$ *00<u>20</u>* peak become higher as the film thickness decreases, indicating that the *c*-axis lattice parameters along the substrate normal decrease. Moreover, the in-plane XRD patterns around $CaBi_4Ti_4O_{15}$ *220* are shown in Fig. 1(c). The $CaBi_4Ti_4O_{15}$ *220* peaks shift toward a lower diffraction angle with decreasing film thickness, suggesting an increase in the in-plane lattice parameter (i.e., the *a*(*b*)-axis).

Figure 2(a,b) plot the out-of-plane *c*-axis and in-plane *a*(*b*)-axis lattice parameters calculated from the diffraction data shown in Fig. 1(a–c) as functions of film thickness, respectively. Additionally, reference data for the $CaBi_4Ti_4O_{15}$ powder are shown[14]. The in-plane XRD measurements confirm that clear peak splitting is not detected for the *200*/*020* peak irrespective of the film thickness because the lattice parameters of the *a*- and *b*-axes are very close in the $CaBi_4Ti_4O_{15}$ crystal lattice (data not shown). The out-of-plane and in-plane lattice parameters for the 780-nm-thick film are almost the same as the reported data for strain-free $CaBi_4Ti_4O_{15}$ powder. As the film thickness decreases, the out-of-plane *c*-axis lattice parameter decreases and drops drastically below 200 nm, whereas the in-plane *a*-axis and *b*-axis lattice parameters increase from 5.42 to 5.46 Å.

To analyse the change in the lattice parameter of $CaBi_4Ti_4O_{15}$ films, Fig. 2(b) also plots the in-plane lattice parameter of the underlying $SrRuO_3$ bottom electrodes obtained from Fig. 1(c) as well as the in-plane lattice parameter of the as-deposited $SrRuO_3$ layer before $CaBi_4Ti_4O_{15}$ film deposition along with the reference data of $Ca_2Nb_3O_{10}$[−20]. The in-plane lattice parameter of $CaBi_4Ti_4O_{15}$ for a 780-nm-thick film is almost equivalent to

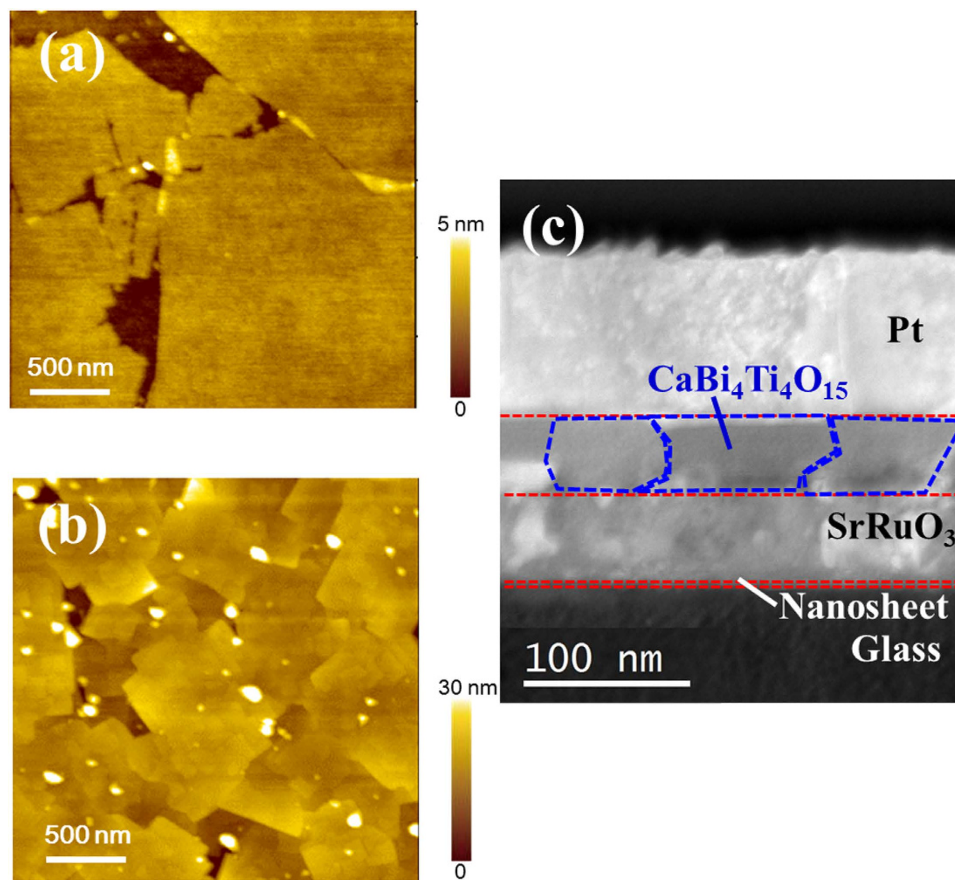

Figure 3. Atomic force microscopy (*AFM*) topographic images of (**a**) $Ca_2Nb_3O_{10}$ nanosheets on glass substrates and (**b**) $CaBi_4Ti_4O_{15}$ films, together with (**c**) cross sectional low-angle annular dark field-scanning transmission electron microscope (LAADF-STEM) images of the films.

that of the $CaBi_4Ti_4O_{15}$ powder, suggesting that the crystal lattice of the 780-nm-thick $CaBi_4Ti_4O_{15}$ film is almost relaxed. Meanwhile, the in-plane lattice parameter of $CaBi_4Ti_4O_{15}$ increases as the film thickness decreases. A similar trend is observed for the in-plane lattice parameters of $SrRuO_3$. It should be noted that the in-plane lattice parameter of $SrRuO_3$ is almost identical to that of the as-deposited 50-nm-thick $SrRuO_3$ films before $CaBi_4Ti_4O_{15}$ deposition but not to that of the $Ca_2Nb_3O_{10}^-$ nanosheets (Fig. 2(b)) because the crystal lattice of the as-deposited $SrRuO_3$ layer is not fully clamped on the lattice of the $Ca_2Nb_3O_{10}^-$ nanosheets. $CaBi_4Ti_4O_{15}$ also possesses a different in-plane lattice parameter from those of the $SrRuO_3$ and $Ca_2Nb_3O_{10}$ nanosheets, indicating that the change in the lattice parameter of $CaBi_4Ti_4O_{15}$ films is not perfectly clamped by the crystal lattice of the underlying $SrRuO_3$ electrode layer. The increase in the in-plane lattice parameter of the $CaBi_4Ti_4O_{15}$ film (Fig. 2(b)) suggests that the in-plane residual strain of $CaBi_4Ti_4O_{15}$ films increases as the film thickness decreases. The large in-plane lattice parameter of thin $CaBi_4Ti_4O_{15}$ is considered to be a response to the larger lattice parameter of the underlying $SrRuO_3$ layer, because the $CaBi_4Ti_4O_{15}$ films are thinner than the 50 nm-thick $SrRuO_3$ layer. Here, as-deposited $SrRuO_3$ films have a larger unit cell than $SrRuO_3$ powders, i.e., a larger in-plane strain, due to the damage occurring under the sputtering process using the present deposition conditions, as reported previously[21,22]. The in-plane lattice parameter of $CaBi_4Ti_4O_{15}$ relaxed and approached the bulk value together with the $SrRuO_3$ layer with the increase in the total thickness.

Figure 3(a,b) shows atomic force microscopy (*AFM*) topographic images of $Ca_2Nb_3O_{10}$ nanosheets on glass substrates and $CaBi_4Ti_4O_{15}$ films. $Ca_2Nb_3O_{10}$ nanosheets have a flat surface with 1–2 units in thickness and 3–10 μm in-plane width. On the other hand, the lateral grain sizes of $CaBi_4Ti_4O_{15}$ films are about 100 nm, which is smaller than the grain sizes of $Ca_2Nb_3O_{10}$ nanosheets. Figure 3(c) shows the cross sectional low-angle annular dark field-scanning transmission electron microscope (LAADF-STEM) image of the films. Dense $CaBi_4Ti_4O_{15}$ films are found to be deposited and their grain sizes look almost identical to those from *AFM* observations.

Dielectric property. Figure 4(a) shows the ε_r for the (001)-oriented $CaBi_4Ti_4O_{15}$ films measured at room temperature and 100 kHz as functions of the film thickness. The ε_r of these films is approximately 210, which is a negligible degradation as the film thickness decreases to 50 nm. This is almost equivalent to the results for epitaxial films[17]. As a reference of ε_r, the ε_r values for $(Ba_{0.7}Sr_{0.3})TiO_3$ films reported by Parker *et al.*, which continuously degrade as the film thickness decreases below 600 nm, are also plotted in Fig. 4(a)[9]. The ε_r value of $(Ba_{0.7}Sr_{0.3})TiO_3$ films becomes smaller than that of $CaBi_4Ti_4O_{15}$ with a film thickness below 80 nm, suggesting that a

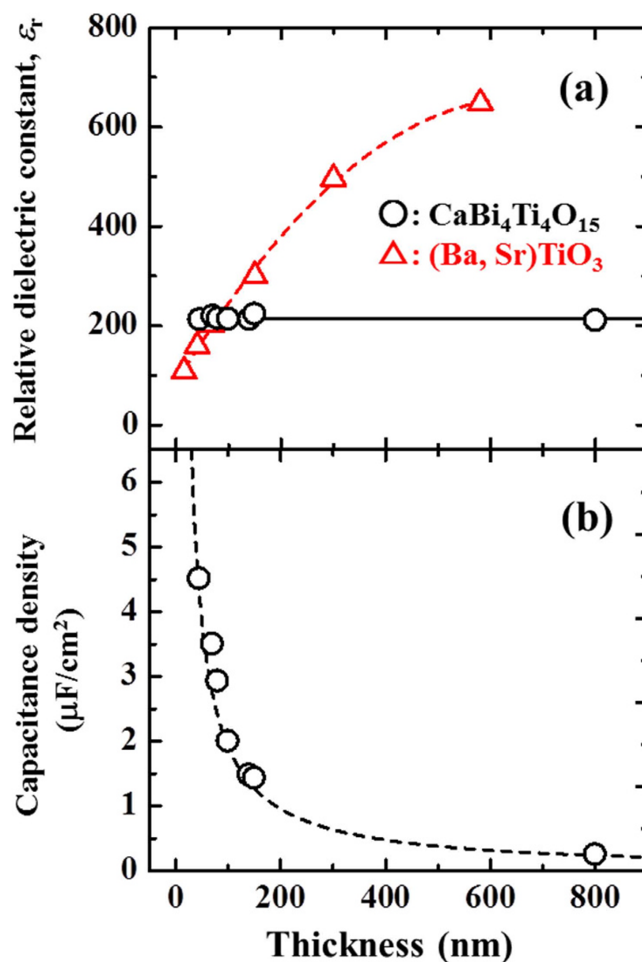

Figure 4. (**a**) Relative dielectric constant (ε_r) and (**b**) capacitance density measured at room temperature as functions of film thickness. (○: $CaBi_4Ti_4O_{15}$; △: $(Ba_{0.7}\,Sr_{0.3})TiO_3$ in ref. 9).

$CaBi_4Ti_4O_{15}$ layer less than 80-nm thick achieves a thin-film capacitor with a higher capacitance density than the conventional $(Ba_{0.7}\,Sr_{0.3})TiO_3$ one.

Figure 4(b) shows the capacitance density at room temperature as a function of film thickness, where the dashed line indicates the estimated data assuming that the $CaBi_4Ti_4O_{15}$ film has an almost constant ε_r value ($\varepsilon_r = 210$, which is equivalent with that of the 780-nm-thick specimen) as the film thickness changes. The theoretical capacitance density is generally proportional to the inverse of the film thickness. The capacitance densities of the obtained (001)-oriented $CaBi_4Ti_4O_{15}$ films are almost identical to the estimated values. As the film thickness decreases, the density increases and reaches a value of $4.5\,\mu F/cm^2$ at a thickness of 50 nm.

It is noteworthy that ε_r remains almost constant despite the increase in the residual strain as the thickness is scaled down to 50-nm (Fig. 2). Thus, we confirm that ε_r of the (001)-oriented $CaBi_4Ti_4O_{15}$ films is free from the size-effect of the capacitance. This is an important feature not only for epitaxial (001)-oriented BLSD films, as already mentioned, but also for uniaxially (001)-oriented ones.

Figure 5 shows the frequency dependencies of the capacitance density and dielectric loss, tan δ, measured from room temperature to 400 °C for 70 and 140 nm-thick $CaBi_4Ti_4O_{15}$ films. The capacitance density is almost independent of the measurement frequency from 100 to 10 kHz irrespective of the measurement temperature up to 400 °C. On the other hand, tan δ decreases with increasing measurement frequency from 100 to 10 kHz, but increases again above 10 kHz for 70 nm thick films as shown in Fig. 5(a). The relatively large dielectric loss at low frequency may originate from the leakage of the capacitor. The tan δ value increases as the measurement temperature increases due to the contribution from leakage current. However, the tan δ of 140 nm thick films remains at a low value below 4%, almost independent of the frequency from 10 to 10 kHz, even at the highest measurement temperature of 400 °C, as shown in Fig. 5.

It must be mentioned that no noticeable peel-off of $CaBi_4Ti_4O_{15}$ films was detected, either in the case of as-deposited films or in the case of films at the highest measurement temperatures of up to 400 °C irrespective of the film thickness.

Figure 6 plots the temperature dependence of the capacitance density and tan δ for (001)-oriented $CaBi_4Ti_4O_{15}$ films with different thicknesses. The capacitance density of these films has a negative slope versus temperature, but shows a small temperature coefficient of capacitance (*TCC*, $TCC \equiv \frac{\Delta\varepsilon_r}{\varepsilon_{r\,(R.\,T.)}} \cdot \frac{1}{\Delta T}$, which is based on the defini-

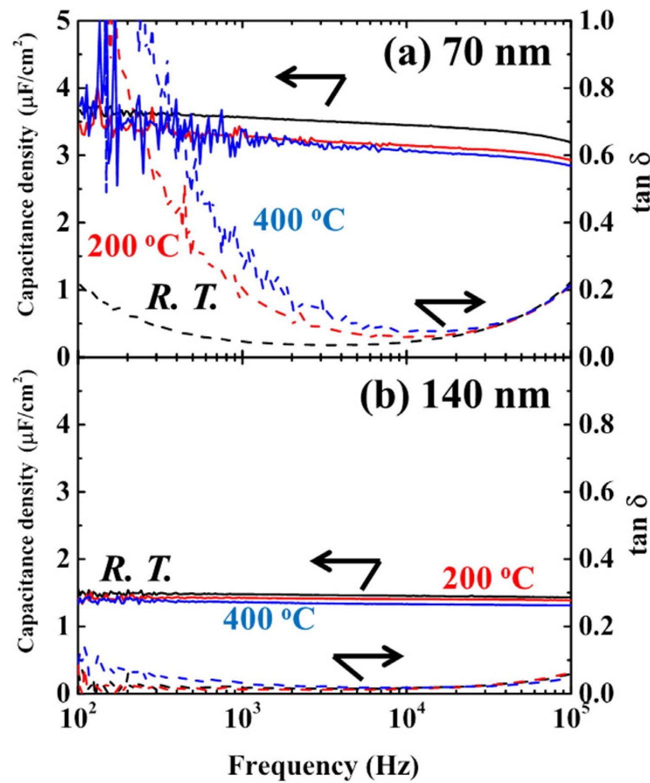

Figure 5. Frequency dependencies of the capacitance density and dielectric loss, tan δ, measured from room temperature to 400 °C for (**a**) 70 and (**b**) 140 nm-thick $CaBi_4Ti_4O_{15}$ films.

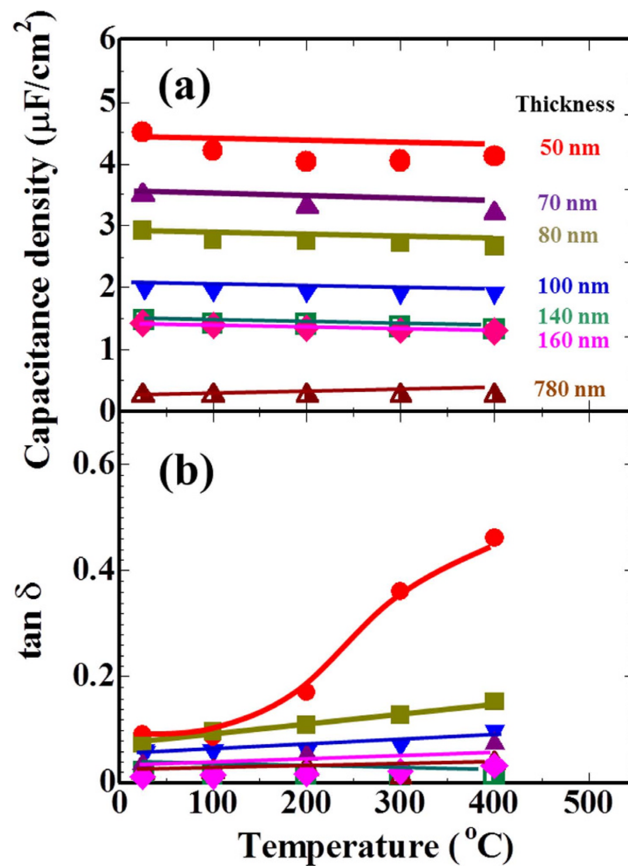

Figure 6. Capacitance density (**a**) and dielectric loss (tan δ) (**b**) of the films as a function of temperature.

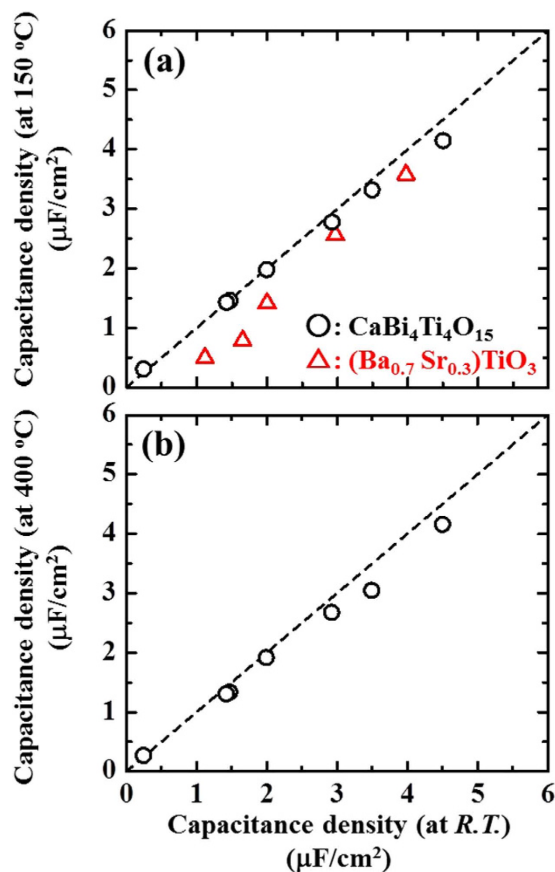

Figure 7. Relationships between the capacitance densities for the films measured at room temperature and (**a**) 150 °C and (**b**) 400 °C. (○: $CaBi_4Ti_4O_{15}$; △: $(Ba_{0.7}\ Sr_{0.3})TiO_3$ in ref. 9).

tion of the Electronic Industries Alliance) in the temperature range from 25 to 400 °C regardless of film thickness down to 50 nm[23]. These *TCC* values fall within the range from −350 to −120 ppm/°C; this characteristic is almost equivalent to that of the epitaxial films in our previous work[11]. These results imply that uniaxially (001)-oriented $CaBi_4Ti_4O_{15}$ films with an in-plane random crystal orientation have dielectric and insulating properties with a small temperature dependence similar to epitaxial films. The capacitance density increases with decreasing film thickness for all temperature regions (Fig. 6(a)). On the other hand, the tan δ value increases with the temperature due to the increase of the leakage current, as shown in Fig. 6(b). However, it decreases with increasing film thickness, especially if it is below 10% up to 400 °C for the films above 100 nm in thickness.

To analyse the effect of thickness on the capacitance density at elevated temperatures, Fig. 7(a) compares the capacitance densities for (001)-oriented $CaBi_4Ti_4O_{15}$ films measured between 150 °C and room temperature. The dashed line indicates the case without a degraded capacitance density up to 150 °C. The measured data are almost located on the dashed line, indicating a negligible difference in the capacitance change between these two temperatures. Figure 7(a) also plots the data for $(Ba_{0.7}\ Sr_{0.3})TiO_3$ films as a reference; as the temperature increases to 150 °C, the capacitance density for thicker films drastically decreases and has a negative *TCC* value[9]. In addition, Fig. 7(b) compares the capacitance densities at 400 °C and room temperature. The measured data are also located for (001)-oriented $CaBi_4Ti_4O_{15}$ films on the dashed line even at temperatures as high as 400 °C. The estimated degradations of the capacitance density from room temperature to 150 and 400 °C are 7% and 9% for 50-nm-thick $CaBi_4Ti_4O_{15}$ films, respectively. Unlike conventionally investigated $(Ba_{0.7}\ Sr_{0.3})TiO_3$ films where the capacitance decreases to 55% between room temperature and 150 °C, the capacitance density for uniaxially (001)-oriented $CaBi_4Ti_4O_{15}$ films shows a small degradation as the temperature increases to 400 °C. These results suggest that (001)-oriented $CaBi_4Ti_4O_{15}$ films produced using $Ca_2Nb_3O_{10}^-$ nanosheet seed layers are novel candidates for high-temperature adaptive capacitor applications due to the superior temperature stability of their electric properties up to 400 °C along with their high capacitance density, which is derived from the small "size effect" upon scaling down the film thickness.

Summary. Uniaxially (001)-oriented $CaBi_4Ti_4O_{15}$ films with various film thicknesses were prepared on $(100)_c SrRuO_3/Ca_2Nb_3O_{10}^-$ nanosheets/glass substrates. All films exhibited a (001) single orientation along the substrate surface normal, but had a random in-plane orientation. The continuous increase in the residual tensile strain as the film thickness decreases leads to a reduction in the out-of-plane "*c*-axis" lattice parameters and an increase in the in-plane "*a*- and *b*-axes" ones. However, the change in ε_r is unremarkable as the film thickness decreases to 50 nm. Consequently, the monotonous increase in the capacitance density is proportional

to the inverse of the film thickness. The capacitance densities of the obtained films show small *TCC* values up to a temperature of 400 °C and are almost independent of film thickness between 50 and 780 nm. By contrast, conventional (Ba, Sr)TiO_3-based films do not exhibit these behaviours. These results indicate that uniaxially (001)-oriented $CaBi_4Ti_4O_{15}$ thin films prepared on $Ca_2Nb_3O_{10}^-$ nanosheet–buffered substrates have potential in high-temperature capacitor applications.

Methods

Uniaxially (001)-oriented $CaBi_4Ti_4O_{15}$ films with various film thicknesses were prepared on $(100)_c SrRuO_3$/($Ca_2Nb_3O_{10}^-$ nanosheets)/glass substrates. The $CaBi_4Ti_4O_{15}$ and about 50 nm-thick $SrRuO_3$ layers were fabricated on ($Ca_2Nb_3O_{10}^-$ nanosheets)/glass (Corning#1737) by the RF-magnetron sputtering method at substrate temperatures of 600 and 550 °C, respectively. The 1–2 unit-thick $Ca_2Nb_3O_{10}^-$ nanosheet layers were coated onto glass substrates by the Langmuir-Blodgett process[20,24,25]. We chose $CaBi_4Ti_4O_{15}$ as the dielectric layer because its high Curie temperature of 790 °C enables a small temperature dependence of the capacitance at elevated temperatures. The deposition time controlled the $CaBi_4Ti_4O_{15}$ film thickness between 50 and 780 nm. Details of the deposition are described elsewhere[11]. After preparing circular Pt top electrodes (100 $\mu m\phi$) by electron-beam deposition, the Pt/$CaBi_4Ti_4O_{15}$/$SrRuO_3$ capacitors were annealed at 400 °C for 30 min under O_2 gas flow.

The constituent phase and crystal orientation of the deposited films were identified by X-ray diffraction (XRD) using a Philips X'pert MRD with Cu $K\alpha$ radiation. The residual strain state was also estimated by in-plane XRD measurements using a Rigaku Smart-lab diffractometer with Cu $K\alpha$ radiation. The electrical properties under various temperatures were measured using an impedance analyser (HP4194A, Agilent) and a sample-heating stage.

References

1. Nishikawa, J., Hagiwara, T., Kobayashi, K., Mizuno, Y. & Kishi, H. Effect of microstructure on the Curie temperature in $BaTiO_3$-Ho_2O_3-MgO-SiO_2. *Jpn. J. Appl. Phys.* **46,** 6999–7004 (2007).
2. Simon, P. & Gogotsi, Y. Materials for electrochemical capacitors. *Nature Mater*. **7,** 845–854 (2008).
3. Simon, P. & Gogotsi, Y. Capacitive energy storage in nanostructured carbon–electrolyte systems. *Acc. Chem. Res.* **46,** 1094–1103 (2013).
4. Almeida, P. S., Soares, G. M., Pinto, D. P. & Braga, H. A. C. Integrated SEPIC buck-boost converter as an off-line LED driver without electrolytic capacitors. *Proc. IECON* **2012,** 4551–4556 (2012).
5. Smolenskii, G. A. & Rozgachev, K. I. Dielectric properties of solid solutions in the system of barium titanate–strontium titanate. *Zh. Tekh. Fiz*. **24,** 1751–1760 (1954).
6. Kang, D.–S., Han, M.–S., Lee, S.–G. & Song, S.–H. Dielectric and pyroelectric properties of barium strontium calcium titanate ceramics. *J. Eur. Ceram. Soc.* **23,** 515–518 (2003).
7. Cockbain, A. G. & Harrop, P. J. The temperature coefficient of capacitance. *J. Phys. D: Appl. Phys*., **1,** 1109–1115 (1968).
8. Huang, Y.-L., Lee, Y.-C., Tsai, D.-C., Yeh, Y.-Y. & Shieu, F.-S. A. Study of low-temperature sintering of $(Ba_{0.6} Sr_{0.4})(Ti_{0.94} Cu_{0.06})O_3$ ceramics with B_2O_3 addition. *Ferroelectrics* **434,** 147–156 (2012).
9. Parker, C. B. , Maria, J.-P. & Kingon, A. I. Temperature and thickness dependent permittivity of (Ba, Sr)TiO_3 thin films. *Appl. Phys. Lett.* **81,** 340–342 (2002).
10. Lee, B. T. & Hwang, C. S. Influences of internal intrinsic low-dielectric layers on the dielectric properties of sputtered (Ba, Sr)TiO_3 thin films. *Appl. Phys. Lett.* **77,** 124–126 (2000).
11. Kimura, J. *et al.* Temperature and electric field stabilities of dielectric and insulating properties for c-axis-oriented $CaBi_4Ti_4O_{15}$ films. *J. Appl. Phys.* **114,** 027002-1-027002–7 (2013).
12. Aurivillius, B. Mixed bismuth oxides with layer lattice. 1. The structure type of $CaNb_2Bi_2O_9$. *Ark. Kemi*. **1,** 463–480 (1949).
13. Aurivillius, B. Mixed Bismuth oxides with layer lattice. 1. The structure type of $Bi_4Ti_3O_{12}$. *Ark. Kemi*. **1,** 499–512 (1949).
14. Kennedy, B. J., Zhou, Q., Ismunandar, Kubota, Y. & Kato, K. Cation disorder and phase transitions in the four-layer ferroelectric Aurivillius phases $ABi_4Ti_4O_{15}$ (A=Ca, Sr, Ba, Pb). *J. Solid State Chem.* **181,** 1377–1386 (2008).
15. Watanabe, T. & Funakubo, H. Controlled crystal growth of layered-perovskite thin films as an approach to study their basic properties. *J. Appl. Phys.* **100,** 051602-1-051602–11 (2006).
16. Irie, H. & Miyayama, M. Dielectric and ferroelectric properties of $SrBi_4Ti_4O_{15}$ single crystals. *Appl. Phys. Lett.* **79,** 251–253 (2001).
17. Takahashi, K. *et al.* Thickness dependence of dielectric properties in bismuth layer-structured dielectrics. *Appl. Phys. Lett.* **89,** 082901-1-082901–3 (2006).
18. Kojima, T. *et al.* Anisotropic electrical properties in bismuth layer structured dielectrics with natural super lattice structure. *Appl. Phys. Lett.* **101,** 012907-1-012907–4 (2012).
19. Shibata, T., Fukuda, K., Ebina, Y., Kogure, T. & Sasaki, T. One-nanometer-thick seed layer of unilamellar nanosheets promotes oriented growth of oxide crystal films. *Adv. Mater.* **20,** 231–235 (2008).
20. Ma R. & Sasaki, T. Nanosheets of Oxides and Hydroxides. Ultimate 2D charge-bearing functional crystallites. *Adv. Mater.* **22,** 5082–5104 (2010).
21. Takahashi, K. *et al.* Thermal stability of $SrRuO_3$ bottom electrode and electric property of Pb(Zr,Ti)O_3 thin film deposited on $SrRuO_3$. *Jpn. J. Appl. Phsy*. **41,** 6873–6876 (2002).
22. Takahashi, K. *et al.* Effect of strain in epitaxially grown $SrRuO_3$ thin films on crystal structure and electric properties. *Jpn. J. Appl. Phsy*. **41,** 5376–5380 (2002).
23. Sun, C., Wang, X., Ji, A. & Li, L. Low-temperature sintering of negative-positive-zero-type temperature-stable ceramics with ZnO-B_2O_3 flux and $SrCO_3$ additive. *Jpn. J. Appl. Phys.* **50,** 081501-1-081501–4 (2011).
24. Osada, M. & Sasaki, T. Two-dimensional dielectric nanosheets: novel nanoelectronics from nanocrystal building blocks. *Adv. Mater.* **24,** 210–228 (2012).
25. Li, B.-W. *et al.* Engineered interfaces of artificial perovskite oxide superlattices via nanosheet deposition process. *ACS Nano* **4,** 6673–6680 (2010).

Acknowledgements

This work was partially funded by the MEXT Elements Strategy Initiative to Form Core Research Center. This work was partially supported by the Center for Integrated Nanotechnology Support at Tohoku University and the Nanotechnology Network Project of MEXT of the Japanese Government. The authors thank Ms. Yumiko Kodama and Kumiko Suzuki for preparing the samples in the microstructure analysis.

Author Contributions

J.K. mainly contributed to this work. H.F. supervised the project. I.T. and M.M. helped to prepare film samples and analyse the data. T.S. and H.U. discussed the results and helped write the paper. T.S., M.O. and T.S. prepared the $Ca_2Nb_3O_{10}^-$ nanosheets on glass substrates and contributed to the paper. T.K., T.S. and T.K contributed to the microstructure analysis.

Additional Information

Competing financial interests: The authors declare no competing financial interests.

How to cite this article: Kimura, J. *et al.* Thermally stable dielectric responses in uniaxially (001)-oriented $CaBi_4Ti_4O_{15}$ nanofilms grown on a $Ca_2Nb_3O_{10}^-$ nanosheet seed layer. *Sci. Rep.* **6**, 20713; doi: 10.1038/srep20713 (2016).

This work is licensed under a Creative Commons Attribution 4.0 International License. The images or other third party material in this article are included in the article's Creative Commons license, unless indicated otherwise in the credit line; if the material is not included under the Creative Commons license, users will need to obtain permission from the license holder to reproduce the material. To view a copy of this license, visit http://creativecommons.org/licenses/by/4.0/